





A co-simulation approach to the wheel–rail contact with flexible railway track

P. Antunes^{1,2}  · H. Magalhães¹  · J. Ambrósio¹  ·
J. Pombo^{1,3,2}  · J. Costa¹

Received: 30 November 2017 / Accepted: 18 August 2018
© Springer Nature B.V. 2018

Abstract The standard approach to railway vehicle dynamic analysis includes running the vehicle multibody models in rigid railway tracks. The wheel–rail contact, independently of the rolling contact model used, is either handled online or via lookup tables. This traditional approach disregards the coupling effects between the railway vehicle dynamics and the railway track flexibility. In this work the assumption of rigidity of the railway track is relaxed and a finite element model of the complete track, i.e. rails, pads, sleepers, ballast and infrastructure, is used to represent the track geometry and flexibility. A rail–wheel contact model that evaluates the contact conditions and forces is used online. The dynamics of the railway vehicle is described using a multibody methodology while the track structure is described using a finite element approach. Due to the fact that not only the multibody and the finite element dynamic analysis use different integration algorithms but also because the vehicle and track models are simulated in different codes a co-simulation procedure is proposed and demonstrated to address the coupled dynamics of the system. This approach allows us to analyze the vehicle dynamics in a flexible track with a general geometry modeled with finite elements, i.e. including curvature, cant, vertical slopes and irregularities, which is another novel contribution. The methodology proposed in this work is demonstrated in an

✉ J. Ambrósio
jorge.ambrosio@tecnico.ulisboa.pt

P. Antunes
pedro.antunes@tecnico.ulisboa.pt

H. Magalhães
hugomagalhaes@tecnico.ulisboa.pt

J. Pombo
j.pombo@hud.ac.uk

J. Costa
joao.n.costa@tecnico.ulisboa.pt

¹ IDMEC, Instituto Superior Técnico, Universidade de Lisboa, Av. Rovisco Pais, 1, 1049-001 Lisbon, Portugal

² University of Huddersfield, Huddersfield, UK

³ ISEL, IPL, Lisbon, Portugal

application, in which the railway vehicle–track interaction shows the influence of the vehicle dynamics on the track dynamics and vice versa.

Keywords Rolling contact · Multibody vehicle model · Flexible track · Railway dynamics · Online contact detection

1 Introduction

The development of computer resources favored numerical dynamic analysis methods to become an essential part of the design and research process of railway systems. The quest for novel solutions to answer the increasing demands for network capacity, either by increasing the traffic speed or the axle loads, put pressure on the existing infrastructures that find in the computational analysis of potential solutions a tool for their virtual testing. The European Strategic Rail Research Agenda [1] and the European Commission for Transports white papers [2] have identified these topics as key scientific and technological priorities for rail transport over the next 20 years. One of the points emphasized is the need to reduce the cost of approval for new vehicles and infrastructure products with the introduction of virtual certification. Certainly, an important issue arising during the design phase of new railway vehicles is the improvement of their dynamic performance. The concurrent use of different computational tools allows carrying several simulations, under various scenarios, to reach optimized designs. Studies to evaluate the impact of design changes or failure modes risks can be performed in a much faster and less costly way than the physical implementation and test of those changes in real prototypes.

Current computer codes for railway applications use specific methodologies that, in general, either handle the vehicle dynamics on a rigid track or deal with moving loads on a flexible track. By analyzing such phenomena independently, it is not possible to capture all the dynamics of the complete railway system and relevant coupling effects. However, developing innovative and more relevant comprehensive methodologies, in a co-simulation environment, allows us not only to integrate all physical phenomena, but also to assess their cross-influence. Co-simulation procedures form a generalist approach of simulating coupled systems on a time-depended basis [3–5]. As the dynamic analysis of multi-disciplinary models is often composed by sub-systems, co-simulation exploits this modular structure by addressing each sub-system with its own distinct formulation and time integration method. Co-simulation approaches avoid the use of a unique and complex formulation with a unified time integration method that compromises the accuracy of the dynamic analysis of each sub-system, consequently becoming computationally expensive and time intensive. A wide range of applications use efficiently co-simulation to couple systems with different formulations, i.e. multidisciplinary problems [6–13]. There are also applications where co-simulation is employed to improve computational performance by allowing parallel computation [14, 15], or establishing active control on mechatronic systems [16, 17], or enabling the use of third party applications [18]. In the realm of railway numeric analysis tools, co-simulation implementations are seldom found. One existing application case is the analysis of the pantograph–catenary interaction, in which a co-simulation procedure has been developed with a finite element catenary model interacting with a multibody pantograph model [19–21]. Also, in the framework of railway vehicle dynamics, a co-simulation approach is used to set active control on vehicle models with tilting [22, 23].

The work presented here purposes a co-simulation procedure for the dynamic analysis of vehicle–track interaction where the main objective is to account for track flexibility in the

dynamic behavior analysis of railway vehicles, which in turn, is reflected on the rolling contact of the rail–wheel interaction. Railway dynamics is a subject where contributions from a wide range of fields are required. Different modeling approaches are used, depending on the objective of the study. The importance of the modeling aspects for the vehicle and track, in the context of their interaction, is related with the frequencies of interest associated to the particular phenomena under study in a state-of-art review by Knothe and Grassie [24]. Although that work mostly focuses on noise and it does not address the track geometry, it already presents some of the important modeling aspects required for flexible tracks to achieve meaningful analysis results. When addressing the vehicle–track interaction, from a perspective of evaluating the dynamic behavior of a railway vehicle, the usual and most popular approach is to model the vehicle using a multibody system formulation and consider the track as a rigid structure [25–27]. This methodology provides acceptable results for dynamic analysis regarding vehicle behavior for ride safety and comfort [28]. These models are adequate to evaluate low frequency dynamic responses such as lateral stability and curving behavior, as most of the high frequency excitation is filtered by the vehicles suspension, up to a certain point. Gialleonardo et al. [29] show that the track flexibility has a significant effect on the evaluation of the vehicle critical speed and in the wheel–rail contact forces. Dynamic effects at mid to high frequency ranges require the introduction of track flexibility [30]. Even in the low frequency domain, track flexibility must be considered when its effects on the railway dynamics are significant, such as when the track is considered to be flawed [31, 32], or switches and crossings are considered [33]. The work by Martínez-Casas et al. [34] shows the importance of considering the flexibility of the railway track, and also of the wheelset, in the interaction between vehicle and track. Although in their work only a single wheelset and a perfect circular track are considered, it can be accepted that the interaction phenomena identified can be expected to be present in more general scenarios. Furthermore, as the wheel–rail contact forces' evaluation depends on the geometry of the wheel and rail, as much as on the relative position between them, track flexibility must be considered when analyzing the development of these rolling contact forces along the track. In scenarios with tangent tracks models, in which modal superposition is used to reduce the size of the finite element track model, Dietz, Hippmann and Schupp [6] present the implementation of a coupled vehicle–track dynamics in a commercial multibody code. Due to the use of a modal representation of the flexible track this approach cannot handle to full dynamics of the system without considering an excessive number of modes for the track, which not only leads to computational inefficiency but also prevents the introduction of nonlinear elements, localized deformations and more general geometries. To this end, the work by Zhai, Wang and Cai [35] demonstrates the importance of considering the coupled vehicle–track dynamics with flexible tracks by developing a simulation scenario, validated experimentally, in which the spatial vehicle multibody model operates on two tracks, one with a large radius and the other with a small radius. However, in all the works cited here, the track geometry is either a tangent track or a curved track with constant radius, a more general, and realistic geometry is never considered.

In this work, a multibody formulation is used to model the railway vehicle and a finite element formulation is presented to model the railway track. To establish the interaction between these models, a novel co-simulation procedure, able to handle the dynamics between the systems, is proposed. This approach allows us to analyze the vehicle dynamics in a flexible track with a general geometry modeled with finite elements, i.e. including curvature, cant, vertical slopes and irregularities, which is another novel contribution that can be used not only to address the running scenarios studied in this work but also to contribute to a number of challenging engineering problems associated to the train–track interaction occurring in tracks with small radius curves, such as squeal noise and short pitch corrugation.

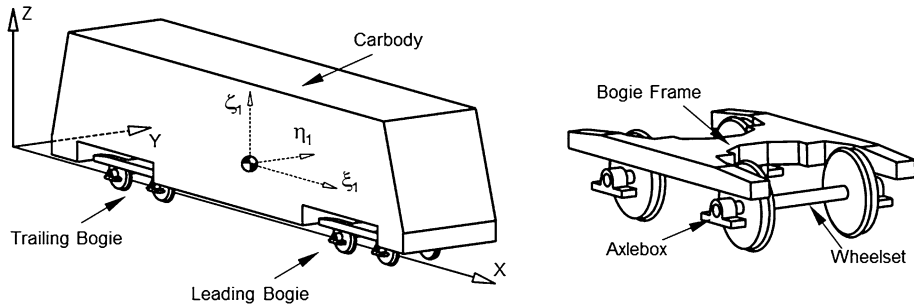


Fig. 1 General multibody model of a railway vehicle

A comparative study on the dynamics of a multibody vehicle with rigid and flexible railway track is presented to appraise the coupled dynamics of the systems and the modification of the rolling contact of the wheel with the track rail.

2 Railway vehicle multibody model

The vehicle multibody model is characterized by a set of rigid and/or flexible bodies that are interconnected by force elements and joints. In turn, a representation of the mechanical elements that constrain the relative motion between structural elements allows modeling the relative mobility of the system components. The equations of motion that represent a multibody model of a railway vehicle, depicted in Fig. 1, are written together with the second time derivative of constraint equations as [36]:

$$\begin{bmatrix} \mathbf{M} & \Phi_q^T \\ \Phi_q & \mathbf{0} \end{bmatrix} \begin{Bmatrix} \ddot{\mathbf{q}} \\ \lambda \end{Bmatrix} = \begin{Bmatrix} \mathbf{g} \\ \gamma \end{Bmatrix} \quad (1)$$

where $\ddot{\mathbf{q}}$ is the vector of the accelerations of the rigid bodies and λ is the Lagrange multiplier vector associated to the joint reaction forces. The remaining terms are described in further detail hereafter.

The multibody model considered in this work comprises a carbody, bogie frames, wheelsets and axleboxes which are modeled as rigid bodies. Their mass and inertial properties are used to form the mass matrix \mathbf{M} . The mechanical joints, in general, are modeled as kinematic constraints, with their modeling parameters being associated to the geometric properties used to form the constraint equations, whose second time derivative includes the Jacobian matrix, Φ_q , and the right-hand side vector, γ . The primary and secondary suspension elements, depicted in Fig. 2, are represented as springs and dampers with appropriate constitutive relations, and the forces transmitted to the connected bodies are included in the force vector, \mathbf{g} . The wheel–rail contact forces are also included in the force vector; their treatment is described in Sect. 4 of this work.

The position and velocity constraint equations are not used explicitly in the integration of the system accelerations and velocities, leading to a drift which results in the violation of these equations as time progresses. It is necessary to eliminate or maintain the violations of the constraint equations under control. The kinematic constraint violations are stabilized using the Baumgarte stabilization method, while kept under prescribed thresholds, or eliminated by using a coordinate partition [37] when they exceed a pre-established value. The

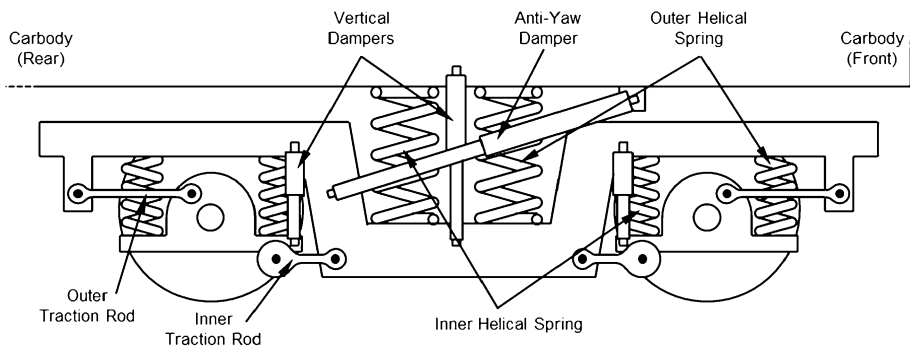


Fig. 2 Suspension system of the railway vehicle

solution of the forward dynamics problem, for the multibody model, is obtained by using a variable time step and variable order numerical integrator [38].

3 Track finite element model and equilibrium equations

The railway track is modeled using the finite element method and its dynamics is analyzed with suitable numerical methods. The ingredients of the finite element model are first described here. They comprise the systematic generation of the finite element model described afterwards. Finally, the equations of motion for the finite element model are presented.

3.1 Finite element components

The railway track is composed of several structural elements: rails, fasteners, rail pads, sleepers, ballast or slab and the sub-structure as depicted in Fig. 3. In this work, the track model is assumed to have only linear deformations and its model is built with linear finite elements. The rails and sleepers are modeled by three-dimensional beam elements, based on Euler–Bernoulli theory [39], the rail pads and fasteners and track supporting layers are modeled with 6 degrees of freedom spring–damper elements. A consistent mass matrix is used for the beam finite elements while a lumped mass description of the inertia is used for other elements in the model.

The rails are modeled with beam elements: 6 elements are used between sleepers to ensure a proper geometry in curves. The sleepers are symmetric and the model of each one is made of 5 beam elements to accommodate transitions of cross-section and/or material properties characteristic of these structural elements. The connection between the sleeper and the rail is modeled using a single spring–damper element with translational stiffness and damping along three perpendicular directions, which represent the sleeper pad and rotational stiffness along the tangent direction of the rail, which is representative of the rail fastening system that prevents the rail from rotating. The track supporting layers are modeled considering two types of spring–damper elements: those connecting the sleepers to the foundation and those connecting two consecutive sleepers. The sleeper-to-foundation connection is represented by the vertical elements below the sleepers, depicted in Fig. 4, and accounts for the flexibility of the supporting layers directly below the sleeper. The sleeper-to-sleeper connection represented by the track-plane elements, connecting the sleepers, as depicted in Fig. 5, accounts for the interlocking action of the supporting structure, i.e. the

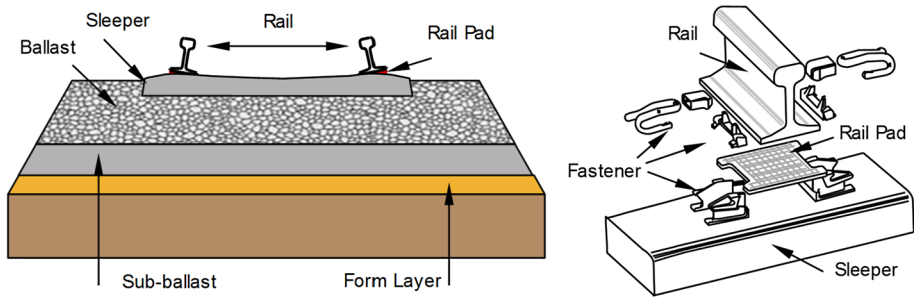


Fig. 3 Typical construction of a railway track with its structural components: (a) track including the ballast and sub-structure, (b) magnified view of the fixation of the rail to the sleeper

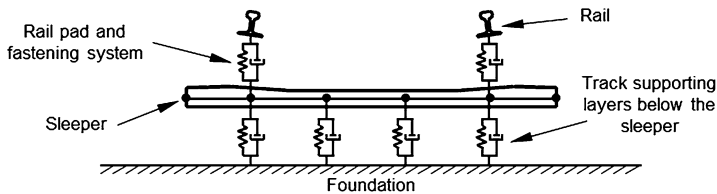


Fig. 4 Cross-section view of the track model

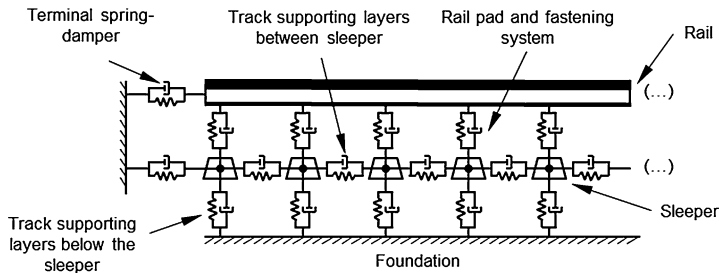


Fig. 5 Longitudinal view of the track model

ballast or the slab. The topology of the track model, with the structural elements considered, is well in-line with the recommendations of Knothe and Grassie [24].

The track supporting layers consider translational stiffness and damping along three perpendicular directions. The foundation is modeled as a fixed “rigid” ground constraining the lower nodes of the track supporting layers finite element mesh. Finally, to avoid the elastic wave reflection characteristic of finite length models intended to represent infinite or very long tracks, massless spring–damper elements are added to the beginning and to the end of the railway track and constrained. This setup corresponds to energy absorption boundary conditions that dissipate the energy associated with the incoming elastic wave thus preventing its reflection, independently of the track length considered in each particular model of the track. The effectiveness of the absorption boundary conditions is achieved by selecting proper damping characteristics for the terminal spring–damper elements the elastic wave reflection is prevented.

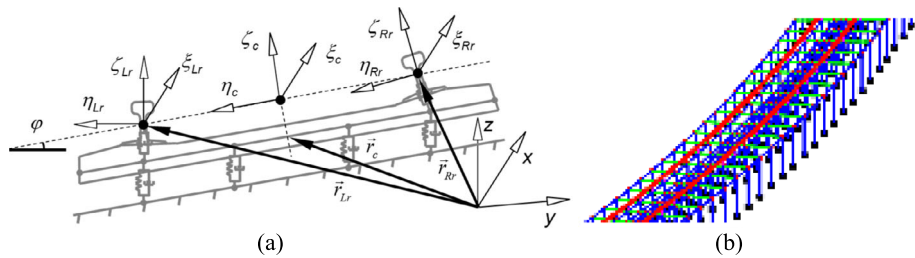


Fig. 6 Elements of the finite element mesh of the track: (a) position coordinates and local reference frame of the track and rails, (b) finite element mesh for the railway track

3.2 Systematic generation of the track finite element model

The track geometrical description, based on the motion of a Frenet–Serret frame of the rails centerline curve, is the basis of the finite element model construction used here [40, 41]. The information necessary to define the railway track centerline geometry, and the local plane in which the track must lay, is obtained from the curvature, cant and elevation information available for the description of the track geometry. The geometry and position of the rails is obtained from the track centerline geometry, taking into account the gauge and the rail geometry, using the track moving frame, as illustrated in Fig. 6.

Using the geometric description of the left and right rails, as a function of their arc length, the position of the nodes of the rails, \mathbf{r}_{Lr} , \mathbf{r}_{Rr} , are defined, as well as the local nodal coordinate frames $(\xi_{Lr}, \eta_{Lr}, \zeta_{Lr})$ and $(\xi_{Rr}, \eta_{Rr}, \zeta_{Rr})$, for the left and right rails, respectively. The finite element mesh of the track includes nodes placed in planes for which the tangent vector to the track centerline is normal and spaced in such a way, along the centerline arc-length, that they include the sleepers, pads and fasteners, such as in the case illustrated in Figure 6(a). In this case, there are two nodes associated with the rail cross-section center, six nodes along the sleepers to enable modeling monoblock, twin-block and timber sleepers, and four nodes for the track foundations. In-between sleepers, there are five rail nodes equally spaced along the rails' curve. The beam finite elements used for the rails have their cross-section oriented according to the local rail referential shown in Figure 6(b). The remaining beam elements, used to model the sleepers depend on their geometry, while the spring–damper elements used to represent the ballast resistance in the tangent-to-track plane and in its vertical direction are set in-between the sleeper nodes and in either the foundation or other sleeper nodes. For more details on the automatic track mesh construction, the interested reader is directed to the work by Costa [42].

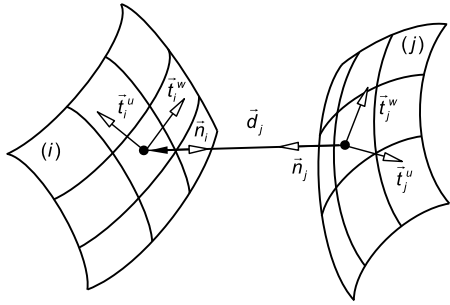
3.3 Equations of motion of the track finite element model

The dynamic equilibrium equations of a railway track are assembled and written as [43, 44]:

$$\mathbf{M}\mathbf{a} + \mathbf{C}\mathbf{v} + \mathbf{K}\mathbf{d} = \mathbf{f}_{\text{track}} \quad (2)$$

where \mathbf{M} , \mathbf{C} and \mathbf{K} are the finite element global mass, damping and stiffness matrices, and \mathbf{a} , \mathbf{v} , \mathbf{d} and \mathbf{f} are the acceleration, velocity, displacement and force vectors, respectively. The global matrices \mathbf{M} , \mathbf{C} and \mathbf{K} are built by assembling the individual finite element matrices, according to the topology of the track mesh. The damping behavior of the beam elements is

Fig. 7 Contact detection between two surfaces [41, 46]



represented using Rayleigh damping [44]. The force vector $\mathbf{f}_{\text{track}}$, containing the sum of all external applied loads, is evaluated at every time step of the integration as

$$\mathbf{f}_{\text{track}} = \mathbf{f}_g + \mathbf{f}_c \quad (3)$$

where \mathbf{f}_g represents the gravitational forces and \mathbf{f}_c represents the equivalent wheel–rail contact forces and moments transferred from the application points to the finite element nodes, as described in detail in Sect. 4.3.

All matrices appearing in the left-hand side of Eq. (2) are constant, for the application scenarios foreseen in this work consequently being linear equations of motion. The dynamic behavior of the track is derived using an integration algorithm based on the implicit Newmark trapezoidal rule [45]. This method is selected due to its unconditional stability, when used implicitly, and its proven robustness in FE applications, as performed in [44].

4 Wheel–rail contact

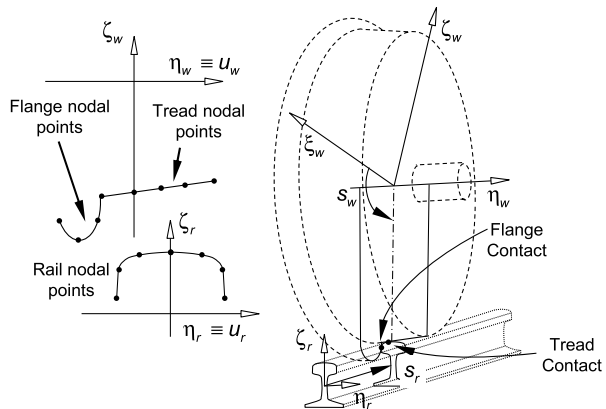
In the vehicle–track co-simulation procedure, the coupling between both sub-systems is associated to the wheel–rail contact. The evaluation of the contact forces requires that the position and velocities of the flexible rail and rigid wheel are known and that a suitable contact force model is used. After evaluating the contact forces, these have to be transferred from their application points to particular points of the model components, i.e. the mass centres of the rigid bodies of the multibody model or the nodes of the finite element model.

4.1 Wheel–rail contact model

The rolling contact problem that characterizes the wheel–rail interaction is solved in two steps: the contact detection, in which the contact points are identified, and the contact force modeling, in which the involved interaction forces are evaluated. The online wheel–rail contact detection method proposed by Pombo et al. [41, 46] is the starting point for the approach proposed here.

The wheel–rail contact detection problem is similar to the contact detection between two parametric surfaces, as those depicted in Fig. 7, described by parameters u_i, w_i, u_j and w_j . The location of the potential contact points in the surfaces must be such that the tangent planes to the surfaces, at those points, are parallel to each other. The surface parallelism

Fig. 8 Identification of the parameters used in the wheel and rail parametric surfaces, including the wheel tread and flange and rail profiles, and surface parameters for the wheel (s_w, u_w) and for the rail (s_r, u_r)



condition is described by the nonlinear system of equations

$$\begin{cases} \mathbf{d}_j^T \mathbf{t}_i^u = 0 \\ \mathbf{d}_j^T \mathbf{t}_i^w = 0 \\ \mathbf{n}_i^T \mathbf{t}_j^u = 0 \\ \mathbf{n}_i^T \mathbf{t}_j^w = 0 \end{cases} \quad (4)$$

where \mathbf{d}_j is the distance vector between the potential points of contact, \mathbf{n}_i and \mathbf{n}_j are the normal vector of surfaces i and j , \mathbf{t}_i^u and \mathbf{t}_i^w are tangential vectors of surface i and \mathbf{t}_j^u and \mathbf{t}_j^w are tangential vectors of surface j , shown in Fig. 7, all defined as functions of the surface parameters.

For each potential contact pair in the wheel–rail contact, i.e. the tread–rail and flange–rail contact pairs, contact exists if

$$\mathbf{d}_j^T \mathbf{n}_i > 0. \quad (5)$$

If contact exists in a particular contact pair, normal and tangential forces are calculated and applied to the bodies in contact at the contact points identified.

The interaction between the wheel and rail is represented by the contact model proposed by Pombo et al. [41, 46]. This model considers that the wheel surface is described by two parametric surfaces, for the tread and for the flange, while the rail is described by a single parametric surface. Therefore, two potential contact points may develop between the wheel and rail, the tread–rail and the flange–rail contact points shown in Fig. 8.

The wheel profile is defined by two sets of nodal points, one for the tread and the other for the flange profile. These nodal points are interpolated to define the cross-section of the wheel profile, as a function of parameter u_w , which in turn is rotated about the wheel axis η_w , with the angle s_w starting from ξ_w , to form the parametric surface of revolution that defines the geometric shape of the wheel. The rail profile is also obtained by the interpolation of another set of nodal points, which are interpolated to define the rail cross-section, as a function of parameter u_r , which, in turn, is swept along the rail arc with the length of the sweep being defined by the arc-length s_r , starting from the origin of the rail. Consequently, the parametric surfaces of the wheel tread and flange and of the rail, depicted in Fig. 8, are fully described by parameters s_w, u_w, s_r and u_r that play the role of parameters u_i, w_i, u_j and w_j in Eq. (4).

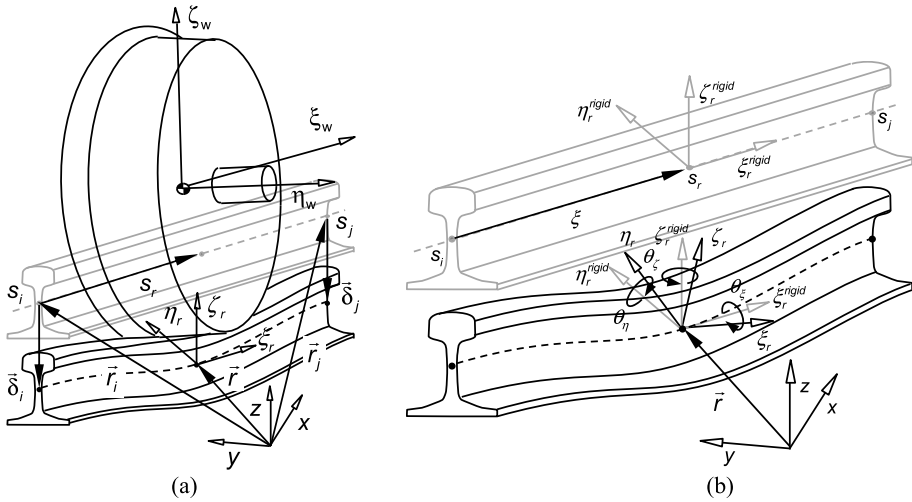


Fig. 9 Deformation of the rail due to the wheel contact: **(a)** displacement of the rail cross-section that includes the contact point, **(b)** rotation of the rail cross-section

The effect of the flexibility of the track on the rail position and orientation is graphically shown in Fig. 9(a), where a rail finite element is displaced with respect to its initial position, in grey, and for which the cross-sections are rotated relatively to their initial orientations. Let the finite element in which wheel–rail contact occurs connect node i to node j , as shown in Fig. 9(a). The position and orientation of the centre of the rail cross-sections in the beam finite element are related to the initial geometry, finite element nodal displacements and shape functions by

$$\begin{aligned} \begin{Bmatrix} \mathbf{r}_r \\ \boldsymbol{\theta}_r \end{Bmatrix} &= \begin{Bmatrix} \mathbf{r}(s_r) \\ \mathbf{0} \end{Bmatrix} + \begin{bmatrix} \mathbf{A}_e & \mathbf{A}_e \end{bmatrix} \begin{bmatrix} \mathbf{N}_i^{dd}(\xi) & \mathbf{N}_i^{d\theta}(\xi) & \mathbf{N}_j^{dd}(\xi) & \mathbf{N}_j^{d\theta}(\xi) \\ \mathbf{N}_i^{\theta d}(\xi) & \mathbf{N}_i^{\theta\theta}(\xi) & \mathbf{N}_j^{\theta d}(\xi) & \mathbf{N}_j^{\theta\theta}(\xi) \end{bmatrix} \\ &\times \begin{bmatrix} \mathbf{A}_e & \mathbf{A}_e & \mathbf{A}_e & \mathbf{A}_e \end{bmatrix}^T \begin{Bmatrix} \delta_i \\ \boldsymbol{\theta}_i \\ \delta_j \\ \boldsymbol{\theta}_j \end{Bmatrix} \end{aligned} \quad (6)$$

where $\mathbf{r}(s_r)$ is the position of the centre of the rail cross-section that includes the contact point for the rigid track, as described by Pombo et al. [41, 46], δ_i and δ_j the nodal displacements, $\boldsymbol{\theta}_i$ and $\boldsymbol{\theta}_j$ the nodal rotations, all expressed in the inertia frame coordinates, \mathbf{A}_e is the finite element transformation matrix from local to global coordinates, and \mathbf{N}^{dd} , $\mathbf{N}^{d\theta}$, $\mathbf{N}^{\theta d}$ and $\mathbf{N}^{\theta\theta}$ are sub-matrices with the shape functions of the beam element [39]. Equation (6) is a function of $\xi = (s_r - s_i)/(s_j - s_i)$, which is the parametric length coordinate of the finite element in which the contact takes place, with s_r being the arc-length of the rail up to the contact point and s_i and s_j the rail arc-lengths up to nodes i and j , respectively.

Due to rail deformation, the rail cross-sections rotate with respect to their orientation on the rigid track, in such a way that they remain perpendicular to the tangent of the arc line of their centres. The linear beam bending theory is used in the formulation of the linear beam finite elements, with the infinitesimal rotations of a cross-section of the element being given by $\boldsymbol{\theta}_r$ in Eq. (6). The transformation matrix from the rigid rail cross-section frame

$(\xi, \eta, \zeta)_r^{\text{rigid}}$ to the deformed rail cross-section frame $(\xi, \eta, \zeta)_r$, both shown in Fig. 9(b), is given by

$$\mathbf{A}_\theta = \begin{bmatrix} 1 & -\theta_\zeta & \theta_\eta \\ \theta_\zeta & 1 & -\theta_\xi \\ -\theta_\eta & \theta_\xi & 1 \end{bmatrix}. \quad (7)$$

A consequence of the displacement and rotation of the rail cross-section on the wheel tread and flange-to-rail contact searches is that not only the evaluation of vector \mathbf{d}_j in Eq. (4) must take into account the new location of the centre of the cross-section \mathbf{r}_r as given by Eq. (6) but also the rail surface vectors \mathbf{n}_j , \mathbf{t}_j^u and \mathbf{t}_j^w need to be rotated. In the wheel–rail contact formulation with a rigid track by Pombo et al. [41, 46], the normal, bi-normal and tangent vectors of the left and right rails are pre-calculated and included in a table accessed online during the contact search. In the procedure for the flexible track, the original vectors in the rigid track table are rotated by matrix \mathbf{A}_θ , and \mathbf{r}_r is added to the rigid rail position before being used in the contact search algorithm, which is done by solving the system of nonlinear equations

$$\begin{cases} \mathbf{d}_j^T \mathbf{t}_i^u = 0 \\ \mathbf{d}_j^T \mathbf{t}_i^w = 0 \\ \mathbf{n}_i^T \mathbf{A}_\theta \mathbf{t}_j^u = 0 \\ \mathbf{n}_i^T \mathbf{A}_\theta \mathbf{t}_j^w = 0. \end{cases} \quad (8)$$

If Eq. (5) is fulfilled for a particular contact pair, normal and tangential contact forces need to be evaluated. These forces depend on the contact geometry and on the material properties of the wheel and rail. Assuming that the contact between the wheel tread or flange and the rail is non-conformal, the normal contact forces are calculated using a Hertzian contact force model with hysteresis damping given by [47]

$$f_n = K \left(1 + \frac{3(1-e^2)}{4} \frac{\dot{\delta}}{\dot{\delta}^{(-)}} \right) \delta^n \quad (9)$$

where K is the stiffness coefficient, e is the restitution coefficient, n is a constant equal to 1.5 for metals, δ is the amount of interpenetration between the surfaces, $\dot{\delta}$ is the interpenetration velocity, and $\dot{\delta}^{(-)}$ is the relative velocity as impact starts.

The tangential forces are evaluated using the formulation proposed by Polach in which the longitudinal creep, or tangential, force is [48]

$$f_\xi = f \frac{v_\xi}{v_C}, \quad (10)$$

while the lateral creep force is written as

$$f_\eta = f \frac{v_\eta}{v_C} + f_{\eta S} \frac{\phi}{v_C} \quad (11)$$

with f being the tangential contact force caused by longitudinal and lateral relative velocities between the contacting surfaces, generally designated as creepages in rolling contact, v_ξ , v_η and ϕ are the longitudinal, lateral and spin creepages, respectively, in the point of contact, v_C is the modified translational creepage, which accounts the effect of spin creepage, and $f_{\eta S}$ is the lateral tangential force, or creep, caused by spin creepage. The Polach

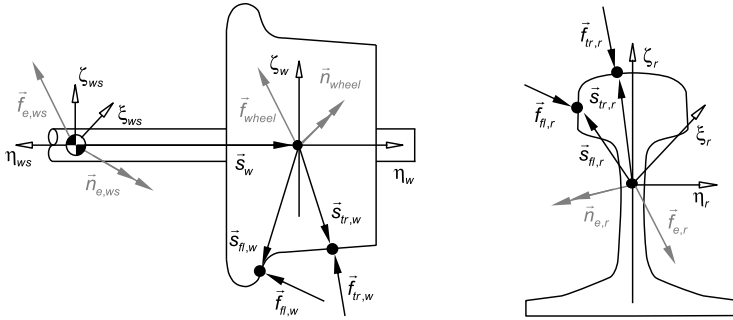


Fig. 10 Wheel and rail contact forces, points of contact and equivalent forces and moments in the wheel centre and in the rail cross-section centre

algorithm requires as input the normal contact force, the semi-axes of the contact ellipse, the combined modulus of rigidity of wheel and rail materials, the friction coefficient and the Kalker creepage and spin coefficients c_{ij} [49].

The contact forces on the wheel tread and flange, shown in Fig. 10 as vectors $\mathbf{f}_{tr,w}$ and $\mathbf{f}_{fl,w}$, respectively, are generically written as

$$\mathbf{f}_{k,w} = f_{k,n} \mathbf{n}_k + f_{k,\xi} \mathbf{t}_{k,w} + f_{k,\eta} \mathbf{t}_{k,u}, \quad k = tr, fl \quad (12)$$

where \mathbf{n}_k is the vector normal to the wheel surface, $\mathbf{t}_{k,w}$ is the tangent vector to the surface in the longitudinal direction of the wheel motion, and $\mathbf{t}_{k,u}$ is the tangent vector in the lateral direction. In turn, the forces $\mathbf{f}_{tr,r}$ and $\mathbf{f}_{fl,r}$ represent the forces applied on the rails, which are opposite to those calculated for the wheels, i.e. $\mathbf{f}_{tr,w}$ and $\mathbf{f}_{fl,w}$.

4.2 Wheel–rail contact model on vehicle

In the multibody model, the information related to the wheel–rail contact forces is added to the force vector \mathbf{g} in Eq. (1), in which all forces are supposed to be applied at the rigid bodies' mass centres, i.e. the origin of the body fixed coordinate systems. The forces due to the wheel–rail contact are applied in the contact points of the wheelset, shown in Fig. 10 for the tread and flange contacts. Therefore, the contact forces are first transferred to the centre of the wheelset by adding all the contact forces to a resultant force and a transport moment due to the transfer of the points of application to the wheel centre, as

$$\begin{aligned} \mathbf{f}_{\text{wheel}} &= \mathbf{f}_{tr,w} + \mathbf{f}_{fl,w} \\ \mathbf{n}'_{\text{wheel}} &= \tilde{\mathbf{s}}'_{tr,w} \mathbf{A}_{ws}^T \mathbf{f}_{tr,w} + \tilde{\mathbf{s}}'_{fl,w} \mathbf{A}_{ws}^T \mathbf{f}_{fl,w} \end{aligned} \quad (13)$$

where $\mathbf{s}'_{tr,w}$ and $\mathbf{s}'_{fl,w}$ are the position vectors of the tread and flange contact points with respect to the wheel centre and expressed in the wheelset body coordinate frame, and \mathbf{A}_{ws} is the transformation matrix from the wheelset body frame to the inertia frame.

In the most common applications, the wheels on the same wheelset are not independent, and consequently they are part of a single rigid body designated by the wheelset. Therefore, the resultant force applied in the wheel mass centre is transferred to the wheelset mass centre, with the resultant force and transport moment on the wheelset being due to the

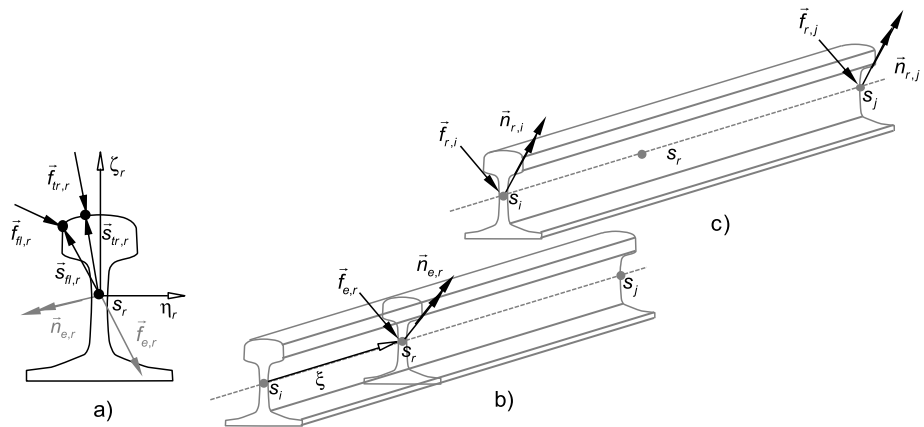


Fig. 11 Wheel–rail contact force: **(a)** rail cross-section in which the wheel tread and flange contact forces are applied, **(b)** equivalent force system in the centre of the cross-section, **(c)** equivalent system of nodal forces in a particular finite element of the rail

wheel–rail contact given by

$$\begin{aligned} \mathbf{f}_{e,ws} &= \mathbf{f}_{\text{wheel}} \\ \mathbf{n}'_{e,ws} &= \tilde{\mathbf{s}}'_w \mathbf{A}_{ws}^T \mathbf{f}_{\text{wheel}} + \mathbf{n}'_{\text{wheel}} \end{aligned} \quad (14)$$

where \mathbf{s}'_w is the position of the wheel centre with respect to the wheelset mass centre, expressed in the wheelset body fixed coordinate system. Thus, the contribution of the wheel–rail contact forces to the force vector \mathbf{g} of Eq. (1) is simply $\mathbf{g}_{e,ws} = [\mathbf{f}_{e,ws}^T, \mathbf{n}_{e,ws}^T]^T$.

4.3 Wheel–rail contact model on track

In a finite element model, lumped forces, such as the wheel–rail contact forces, can be applied on the nodes of the mesh but not in the middle of the element. As seen in Fig. 10, the wheel–rail contact forces are applied on the rail surface, whereas the beam element used in the model for the rail considers only its geometric centre. Therefore, the resultant of the contact forces, $\mathbf{f}_{e,r}$, is applied on the rail cross-section centre and a transport moment, $\mathbf{n}_{e,r}$, shown in Figs. 10 and in 11(a), is added to obtain the equivalent force system in the cross-section centre as

$$\begin{aligned} \mathbf{f}_{e,r} &= \mathbf{f}_{tr,r} + \mathbf{f}_{fl,r} \\ \mathbf{n}_{e,r} &= \tilde{\mathbf{s}}_{tr,r} \mathbf{f}_{tr,w} + \tilde{\mathbf{s}}_{fl,r} \mathbf{f}_{fl,w} \end{aligned} \quad (15)$$

where $\mathbf{s}_{tr,r}$ and $\mathbf{s}_{fl,r}$ are the contact position vectors with respect to the cross-section centre, defining the inertia reference frame coordinates. Note that the transformation of coordinates of the contact position points from rail cross-section to global coordinates is done by $\mathbf{s}_{tr,r} = \mathbf{A}_r \mathbf{s}'_{tr,r}$ and $\mathbf{s}_{fl,r} = \mathbf{A}_r \mathbf{s}'_{fl,r}$ with the transformation matrix $\mathbf{A}_r = [\mathbf{u}_\xi \ \mathbf{u}_\eta \ \mathbf{u}_\zeta]^T_r$.

An equivalent system of forces and moments applied at the beam finite element nodes, shown in Fig. 11, that represents contact forces and transport moment applied to the rail cross-section centre needs to be evaluated. The equivalent nodal forces are related to the

concentrated forces and moments via the shape functions matrix as

$$\begin{Bmatrix} \mathbf{f}_{r,i} \\ \mathbf{n}_{r,i} \\ \mathbf{f}_{r,j} \\ \mathbf{n}_{r,j} \end{Bmatrix} = \begin{bmatrix} \mathbf{A}_e & & & \\ & \mathbf{A}_e & & \\ & & \mathbf{A}_e & \\ & & & \mathbf{A}_e \end{bmatrix} \begin{bmatrix} \mathbf{N}_i^{dd}(\xi) & \mathbf{N}_i^{d\theta}(\xi) & \mathbf{N}_j^{dd}(\xi) & \mathbf{N}_j^{d\theta}(\xi) \\ \mathbf{N}_i^{\theta d}(\xi) & \mathbf{N}_i^{\theta\theta}(\xi) & \mathbf{N}_j^{\theta d}(\xi) & \mathbf{N}_j^{\theta\theta}(\xi) \end{bmatrix}^T \times \begin{bmatrix} \mathbf{A}_e & \\ & \mathbf{A}_e \end{bmatrix}^T \begin{Bmatrix} \mathbf{f}_{e,r} \\ \mathbf{n}_{e,r} \end{Bmatrix} \quad (16)$$

and applied on the finite element nodes, i.e. $\mathbf{f}_{r,i}$ and $\mathbf{n}_{r,i}$ are applied on node i while $\mathbf{f}_{r,j}$ and $\mathbf{n}_{r,j}$ are applied on node j , as shown in Fig. 11(c). The forces and moments are expressed in the inertia coordinate frame coordinates.

5 Vehicle–track co-simulation

The vehicle–track co-simulation procedure, presented here, establishes the interaction between the individual sub-systems, each with its own distinct mathematical formulation and integration methodology, with their dynamic analysis being performed by independent codes eventually able to run in a stand-alone mode. The behavior of the two sub-systems is affected reciprocally by each other. A particular aspect of the proposed co-simulation procedure concerns the synchronization of the integration algorithms that run with independent time steps, with the numerical stability and accuracy of the dynamic analysis of the coupled systems being a fundamental aspect to account for [50].

The proposed co-simulation procedure is based on three main key steps addressed hereafter. The first step is to establish the coupling approach, i.e. an interface between the sub-systems that defines a set of state variables or forces within each sub-system to be shared with the other. The second step is to establish a fast and reliable data exchange procedure for the state variables and forces. The third, and final, step is to build a communication protocol that manages the use of the state variables and contact forces through the integration scheme for both sub-systems during their dynamics analysis.

5.1 Vehicle–track interface

Though the coupling approach depends on the type of interaction between the models, most often the coupling is set by imposing either a kinematic constraint between the models or a set of constitutive interaction laws. Such constitutive interaction laws can result in a set of forces/torques that are applied on each sub-system. In this work, due to the nature of the coupled problem where their interaction is defined by the wheel–rail contact, the coupling of the sub-systems is established by the application of the resulting contact forces/torques on each model. Thus, each computer code solves its own equations of motion, which include the interaction forces. As the wheel–rail contact forces provide the link between to two sub-systems, the evaluation of the contact is done in one of the sub-systems while the other provides the parameters required to make such evaluation possible, in this case the state variables that allow for the solution of the contact problem. Evaluating the wheel–rail contact on the track sub-system, as shown in Fig. 12, avoids a computationally expensive communication scheme. The contact model requires the deformed centre position of the rails, in the neighborhood of the arc length of the track in which contact occurs, s_r , to allow for the solution of the nonlinear Eq. (4) for contact detection, which in turn requires

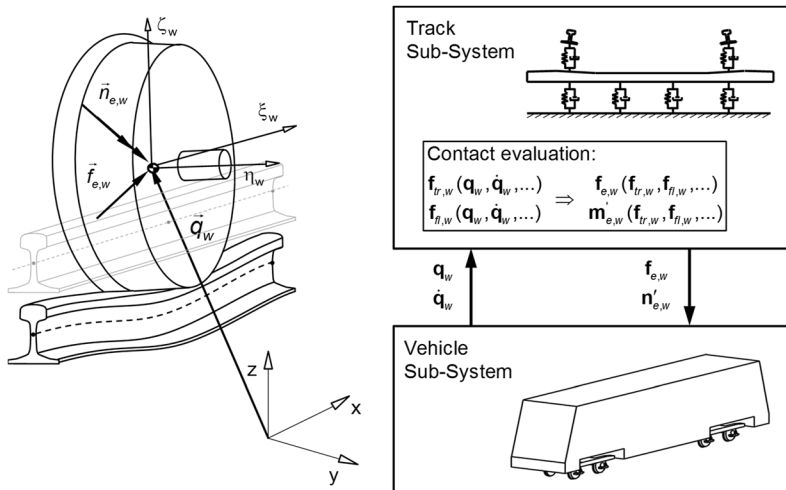


Fig. 12 Vehicle–track co-simulation interface

all information associated to the finite element mesh of the rails already available in the track sub-system. The vehicle sub-system is set to provide the spatial position, \mathbf{q}_w , and velocity, $\dot{\mathbf{q}}_w$, of each wheel centre of the vehicle model. The wheel–rail contact problem is solved in the track sub-system and, in return, the vehicle sub-system receives from the track sub-system an equivalent wheel–rail contact force, $\mathbf{f}_{e,w}$, and transport moment, $\mathbf{n}'_{e,w}$, to be applied at the corresponding wheel centres.

5.2 Data exchange method

As the state variables are a common resource shared between two concurrent processes, the data exchange procedure is critical in the co-simulation. This procedure is not only responsible for exchanging the state variable data between sub-systems but also for controlling their access. This leads to two important requirements that the data exchange method needs to fulfill. First, given the frequency at which data needs to be exchanged, it must be sufficiently fast so that it does not become a bottleneck of the co-simulation procedure. Second, it must be robust by providing a mechanism where both sub-systems are synchronized over time and do not overstep each other.

The data exchange method is built by exchanging two communication files, as depicted in Fig. 13. One file includes the state variables data, composed of the wheel centre position and velocity, denoted by *V2T file*, written by the vehicle sub-system code and read by the track sub-system code. The other file written by the track sub-system code and read by the vehicle sub-system code, denoted by *T2V file*, includes the equivalent wheel–rail contact forces to be applied on the centre of each wheel. In order to keep both sub-systems synchronized and to avoid data to be overwritten without being read first, which is known as a race condition [51, 52], a binary semaphore is implemented [53]. Here, each communication file also carries a binary flag that, according to its value, either gives permission to one sub-system to read the data or the other to write it over. This method not only controls the reading/writing access of the state variables but also provides means to control the progress of the integration algorithms of each one of the individual analysis codes so that they stay synchronized.

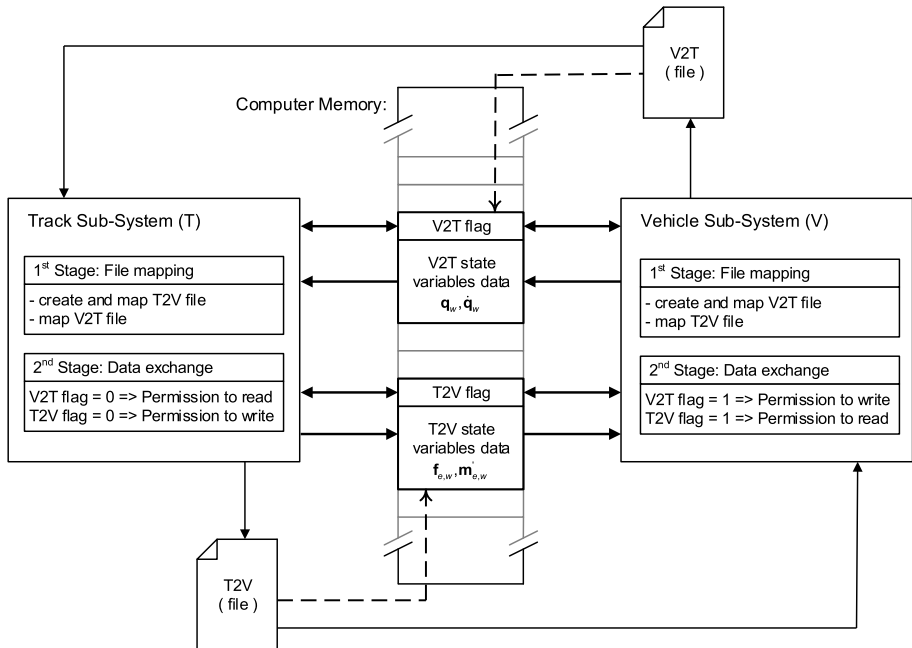


Fig. 13 Vehicle–track data exchange procedure

The time spent on data exchange between codes must be negligible compared to the computation time costs of the independent analyses. Therefore, the data exchange procedure uses memory sharing via memory mapped files. A memory mapped file is a segment of computer memory which is mapped in order to have a direct byte-for-byte assignment to a hard disk file or other resource that the operating system can refer to. Once this correlation is established, or mapped, the memory mapped file can be accessed directly from computer memory, yielding a much faster data exchange process. This memory sharing implementation is depicted in Fig. 13. At the start of the analysis, one of the applications creates a file and maps it to memory while the other waits for the file to be created. Whenever this file is found by the waiting application, the file is also mapped to the same corresponding memory address. Having both applications mapped the same file in memory they can communicate using a common memory address whereas the created file only serves as a point of reference for both applications to map the same dataset in memory.

5.3 Communication protocol

The communication protocol is responsible for managing the use and update of the state variables along the integration scheme of each sub-system. In this work each sub-system has a distinct formulation and integration procedure, on one side the railway multibody vehicle model is evaluated as a nonlinear dynamic system handled with a variable time step, multi-order integrator, while a finite element track model is evaluated as a dynamic linear system integrated with a Newmark family numerical integrator with a fixed time step. The heterogeneity of these integration schemes and the premise to keep them independent and fundamentally unchanged requires careful consideration. Thus, the compatibility between the two integration algorithms imposes that the state variables of the two sub-systems

are readily available at every time step. This is guaranteed by a state variable interpolation/extrapolation scheme where the state variable data used by each sub-system is updated following the communication protocol presented in Fig. 14. At a given time step, t_T , the track model requires the positions and velocities of the wheel centres to evaluate the wheel–rail contact force. Meanwhile, the vehicle model, evaluated with a variable time step, requires the equivalent wheel–rail contact forces available to be applied on its model and proceeds with its integration. Therefore, there is a need of one of the sub-systems to make a prediction on a forthcoming time, before advancing to a new time step. Given the integration procedure structure between the two systems, the vehicle model is selected to be the leading sub-system. Hence, the equivalent contact forces to be applied on the wheel are estimated by linear extrapolation of the state variable data, \mathbf{f}_E , t_E , and provided by the track sub-system. Whenever the track sub-system integrator requires data to proceed, it is set to wait until the vehicle model has advanced to the point where it can interpolate the results of its evaluation in order to provide the wheel positions and velocities for the required time step. It is important to note that the accuracy and stability of this methodology relies on ensuring that the vehicle sub-system variable time step size is never larger than the fixed time step of the track. Furthermore, the vehicle integrator time step size is also required to be small enough so it does not critically overextend the state variable extrapolation. This is guaranteed by limiting its maximum step size to be smaller than the track time step size.

6 Demonstrative application

The demonstration of the vehicle–track co-simulation procedure proposed here, and of its implications on the wheel–rail rolling contact problem, is carried with a case scenario. Three alternatives are tested for the representation of the wheel–rail interaction problem. One corresponds to the co-simulation procedure, presented here, where a multibody vehicle model is coupled with a finite element track model so that track flexibility is taken into consideration. A second alternative consists of the same co-simulation procedure but assuming the track to be rigid by neglecting the finite-element nodal displacements. The third simulation is run, to serve as a control, with the standalone multibody code where the vehicle runs on the rigid track, i.e. using the standard approach in railway vehicle dynamics studies.

6.1 Case scenario

The track considered for the case scenario is composed of a straight segment followed by a small radius left-hand curve and a short straight track segment. It also includes two transition zones between the curve and straight segments as depicted in Fig. 15. The track geometry is designed following standard EN13803-1 for a vehicle operating at a speed of 110 km/s while negotiating a 500 m radius curve at its maximum allowed superelevation and cant deficiency limit. Iberic gauge is selected for the track with UIC60 rail profiles and 1/20 rail inclination.

The material properties used to build the finite element model of the track are presented in Table 1, for the rail and sleeper beam elements, and in Table 2, for the remaining spring–damper elements, with the references in which the data for the parameters is obtained also being provided.

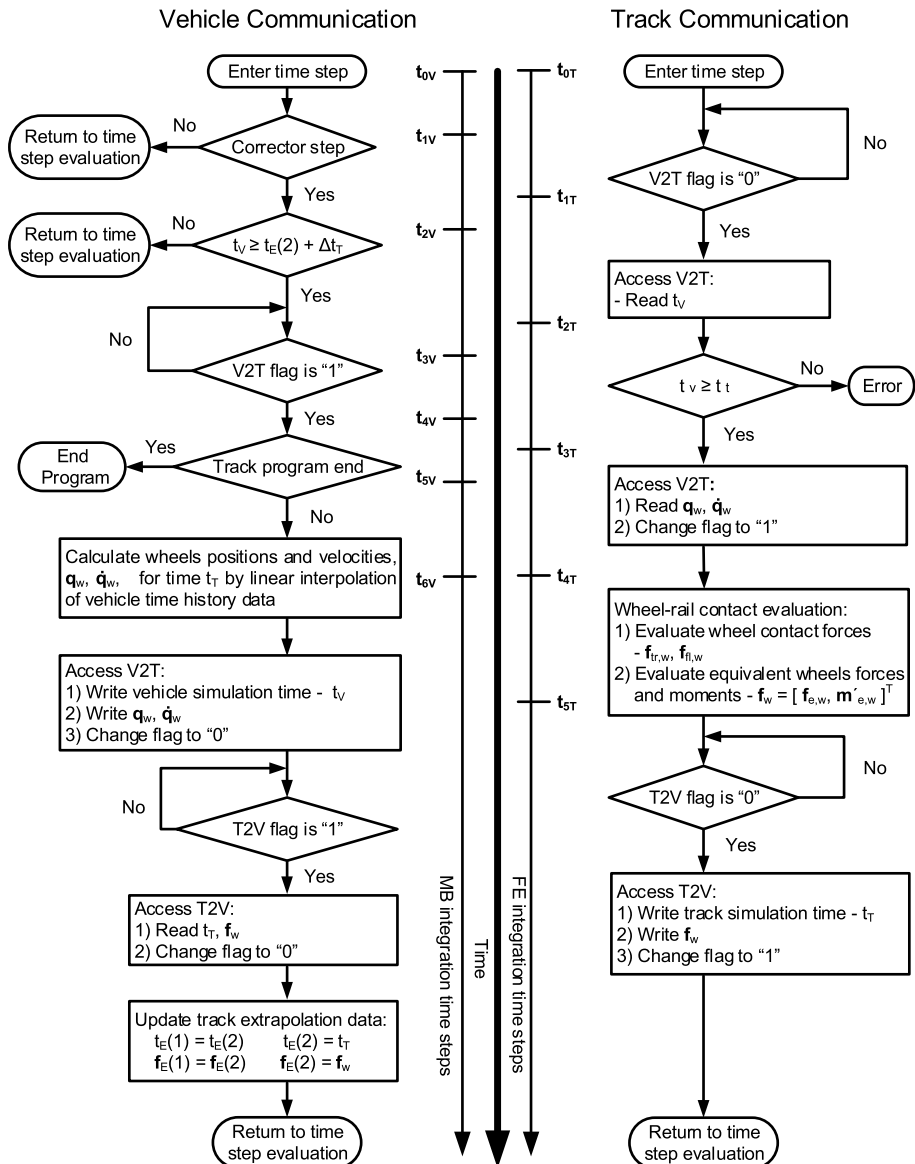


Fig. 14 Vehicle-track communication protocol

The track model, which in the case of this demonstration scenario has a length of 500 m, includes energy absorption boundary conditions at the start and end of the track model. The properties of the spring-damper elements used in the start and end of the track, in the longitudinal direction, are presented in Table 2. It should also be noted that although the values for the parameters used to model the track are obtained from state-of-art references, they do not ensure that the track model dynamic response is that of an existing one. The receptances on the rail above the sleeper and in-between sleepers can be evaluated either to validate the

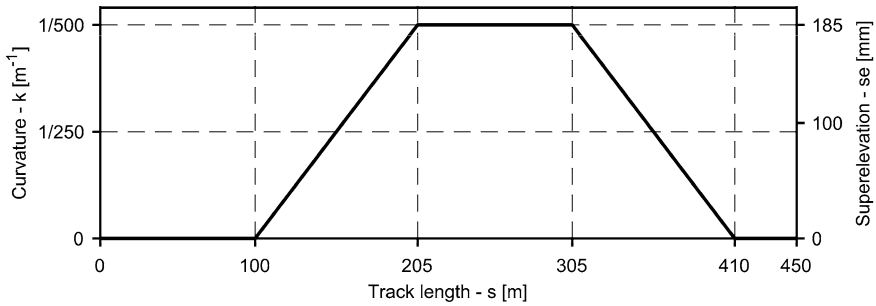


Fig. 15 Curvature and superelevation along track length

Table 1 Beam element properties of the track model

EB beam element properties	Rail	Ref.	Sleeper	Ref.
Young modulus— E [Pa]	2.10×10^{11}	[32]	3.10×10^{10}	[54]
Torsion modulus— G [Pa]	8.08×10^{10}		1.50×10^{10}	[55]
Cross-section area— A [m ²]	7.67×10^{-3}	[56]	5.6×10^{-2}	[54]
Polar moment of area in $\eta\zeta$ plane— $J_{\xi\xi}$ [m ⁴]	3.55×10^{-5}	[56]	1.71×10^{-3}	
Second moment of area in $\xi\zeta$ plane— $I_{\eta\eta}$ [m ⁴]	3.04×10^{-5}	[56]	2.60×10^{-4}	
Second moment of area in $\xi\eta$ plane— $I_{\zeta\zeta}$ [m ⁴]	5.12×10^{-6}	[56]	1.67×10^{-4}	
Density ρ [kg/m ³]	7860	[35]	2750	[32]
Rayleigh damping parameter— α [s ⁻¹]	3.98×10^{-4}		3.98×10^{-4}	
Rayleigh damping parameter— β [s]	0.94		0.94	

Table 2 Spring–damper element properties of the track model

Spring–damper element	Pads	Ref.	Ballast	Ref.	Sleeper interaction	Ref.
Vertical stiffness— K_v [N/m]	1.30×10^8	[57]	6.19×10^7	[58]	5.50×10^5	[59]
Transversal stiffness— K_t [N/m]	4.00×10^7		1.00×10^7	[59]	4.05×10^5	[59]
Longitudinal stiffness— K_l [N/m]	4.00×10^7	[57]	5.50×10^5		3.92×10^7	[35]
Longitudinal rotation stiffness— K_{rl} [N/m]	2.00×10^5		—	—		
Vertical damping— C_v [Ns/m]	1.50×10^5	[57]	2.94×10^4	[35]	2.94×10^4	
Transversal damping— C_t [Ns/m]	1.00×10^5		2.94×10^4		2.94×10^4	
Longitudinal damping— C_l [Ns/m]	1.00×10^5	[57]	2.94×10^4		2.94×10^4	[35]
Lumped mass— m [kg]	—		226.41	[58]	—	

track models against experimental results, if these exist, or to provide typical responses for realistic track models that can be compared with those available in the literature, in particular in the work by Knothe and Grassie [24].

The vehicle model considered in this work is used by a Portuguese railway operator for passenger transport [60, 61]. The initial position of the bodies of the vehicle model, shown in Fig. 1, their masses and inertia properties are listed in Table 3. The primary suspension, responsible for transmitting the forces between the axleboxes and the bogie frame, is shown in Fig. 2, with its kinematic and force element parameters being described in [60, 61]. The

Table 3 Center of mass and inertia properties of the bodies considered in the vehicle model

ID	Body	Center of mass [m] (X/Y/Z)	Mass [kg]	Moment of inertia [kg/m ²] ($\xi\xi/\eta\eta/\zeta\zeta$)
1	Carbody	11.5000/0.000/1.432	46200	78000/2600000/2600000
2	Leading bogie	Bogie frame	3000	2100/2600/4800
3		Front wheelset	1800	900/10/900
4		Front left axlebox	10	1/1/1
5		Front right axlebox	10	1/1/1
6		Rear wheelset	1800	900/10/900
7		Rear left axlebox	10	1/1/1
8		Rear right axlebox	10	1/1/1
9	Trailing bogie	Bogie frame	3000	2100/2600/4800
10		Front wheelset	1800	900/10/900
11		Front left axlebox	10	1/1/1
12		Front right axlebox	10	1/1/1
13		Rear wheelset	1800	900/10/900
14		Rear left axlebox	10	1/1/1
15		Rear right axlebox	10	1/1/1

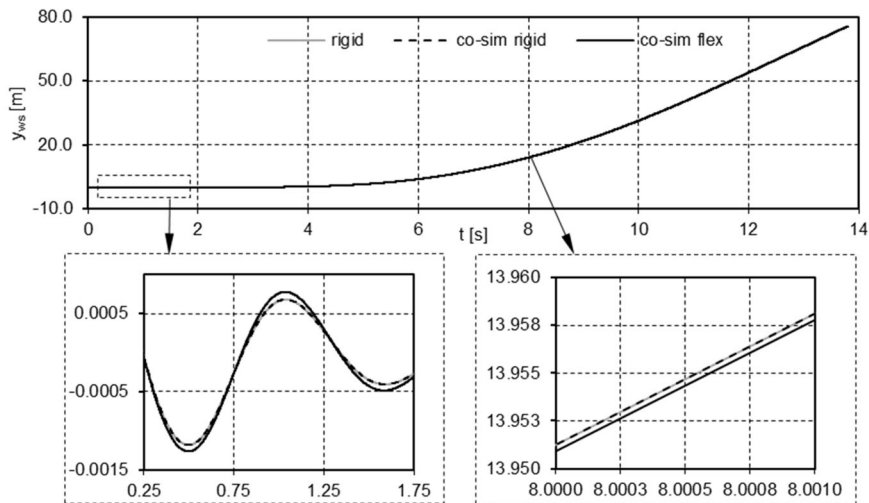


Fig. 16 Comparison of the lateral motion of the leading wheelset

secondary suspension, responsible for transmitting the forces between the bogie frame and the carbody is also shown in Fig. 2, with the data necessary to build its model and the bogie carbody connection being found in [60]. The relative motion between the wheelset and axleboxes is constrained by tapered rolling bearings. Due to the nature and construction of these bearings, it is assumed here that the revolute joints between the wheelset and axleboxes are representative of their relative kinematics [36].

6.2 Results

The vehicle–track interaction dynamics involves a large set of dynamic responses that is not possible to present concisely in this work. With the purpose of presenting the influence of the flexible track on the vehicle dynamics, the interaction forces due to the wheel–rail contact and the kinematics of the front wheelset of the vehicle are selected as representative responses that allow understanding novel features of the approach proposed. In all that follows, the initial 0.25 s of any simulation results are discarded, as during this period the dynamics of the system exhibits a transient response while reaching a steady-state operation. The kinematics of the leading wheelset of the vehicle is presented in Fig. 16 for the lateral position, in Fig. 17 for the attack angle, and in Fig. 18 for the vertical position. Comparing the results between the standalone simulation in which the track is considered rigid, denoted by *rigid*, and the co-simulation with the rigid finite element track model, denoted as *co-sim rigid*, a good agreement is observed, with their maximum absolute deviation being lower than 2.5×10^{-5} m for the lateral motion, and lower than 8×10^{-8} m for the vertical motion. Comparing the results between the standalone simulation in which the track is considered rigid, denoted by *rigid*, and the co-simulation with the rigid finite element track model, denoted as *co-sim rigid*, a good agreement is observed with their maximum absolute deviation being lower than 2.5×10^{-5} m for the lateral motion, $4.7 \times 10^{-4}^\circ$ for the attack angle, and 8×10^{-8} m for the vertical motion. Given that the two simulations consider the rigid track, where one is evaluated in co-simulation, the residual deviation on the results shows that the implemented co-simulation procedure is accurate.

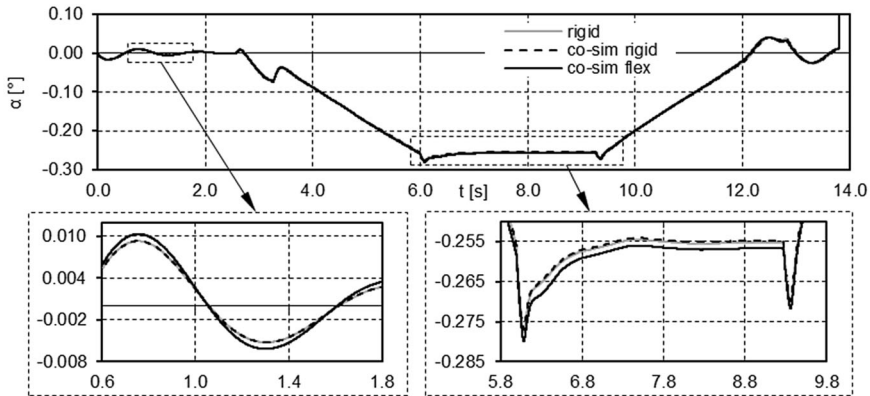


Fig. 17 Comparison of the leading wheelset angle of attack

Comparing the co-simulation results involving the rigid track, *co-sim rigid*, and the flexible track, *co-sim flex*, it is possible to identify a distinguishable influence of the track flexibility on the wheelset motion. With respect to the lateral motion, a slightly higher amplitude of the lateral motion is noticeable in the straight segment of the flexible track simulation. In the curved segment the lateral motion of the wheel also presents small offset from the motion when rigid track is considered. The angle of attack of the evaluated leading wheelset also shows a small influence of the track flexibility, with a slightly larger angle when track flexibility is considered. Moreover, when comparing the vertical motion of the wheelset, in Fig. 18, besides the vertical offset also an oscillatory movement is found in the simulation with track flexibility. This additional oscillatory behavior is more easily identified in the straight segment, whereas in the curve the motion of the wheelset set is also influenced by the wheel flange contact at the outer rail. Note that the frequency of these oscillations is about 51 Hz, which is consistent with the periodicity of the track sleepers, spaced at every 0.6 m, for a vehicle traveling at 110 km/h.

For the standalone simulation with rigid track and the co-simulation with the flexible track, the left and right wheel flange contact forces of the leading wheelset are presented in Fig. 19. Flange contact only occurs in the outer wheel during curve negotiation. The force peaks observed when the wheels enter the transition and the curve segment are smaller when track flexibility is considered. On the curve section, it can also be noted that the flange force is oscillating at a higher amplitude when the track is considered rigid.

The oscillating amplitude and peak differences on the curved segment of the track can also be observed on the lateral and vertical contact forces applied on the wheel. These forces are presented in Figs. 20 and 21, respectively, for the left and right leading wheels of the front bogie. In the curve segment of the track, both the lateral and vertical contact forces of the right wheel are higher. This is due to the flange forces acting on the right wheel when the curve is negotiated. It is also possible to observe two force peaks on the first transition segment from straight to curved track around the time of 2.5 and 3.2 s. These correspond to the instants in which the leading wheels of the front and rear bogies enter the transition zone. Therefore, the wheel–rail contact on the front wheel of the front bogie is sensitive to the contact perceived on the rear bogie. Furthermore, on the straight segment the lateral contact forces from the co-simulation with flexible track are 10% higher than those observed for the rigid track simulation. This difference can be related with the configuration of the deformed track which promotes different wheel–rail contact conditions. It is also of importance to

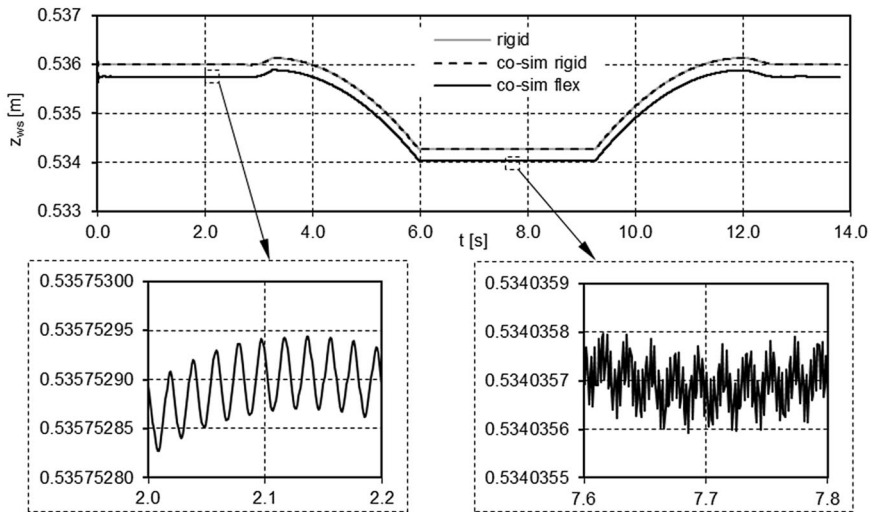


Fig. 18 Vertical motion comparison of the leading wheelset

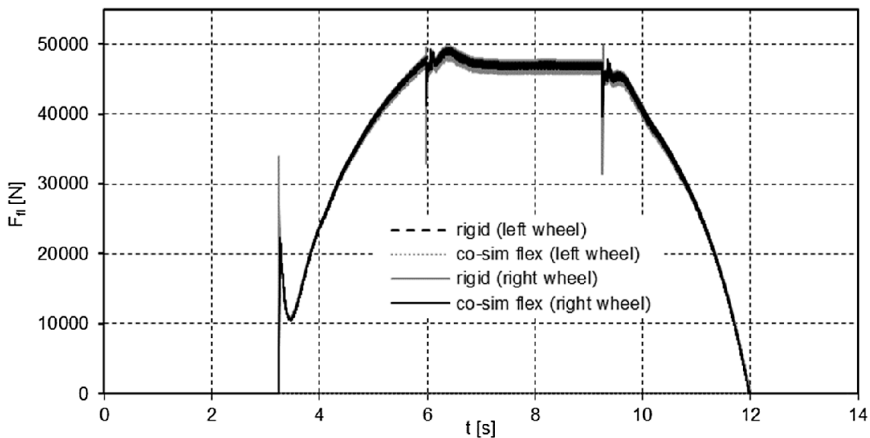


Fig. 19 Flange contact force on the left and right wheel of the leading wheelset

state that although, for the sake of simplicity, the contact forces on the co-simulation with rigid track, *co-sim rigid*, are not shown here, they are similar to those obtained with the standalone multibody code in which only rigid tracks are used.

The effects of the vehicle–track interaction on the flexible track are depicted by the vertical and transversal displacements of the left and right rail at two different cross-sections, presented in Figs. 22 and 23. These figures correspond respectively to the rails displacements evaluated on the straight and curve segment at the 66 and 255 m mark of the track length. The vertical solid lines marked in Figs. 22 and 23 indicate the instants in which the train wheels pass on each mark. The absolute maximum displacement peaks are observed in-between the front and rear wheel passage of each bogie, except for the transversal displacements on the curved segment. This relates to the contact on the wheel flange that

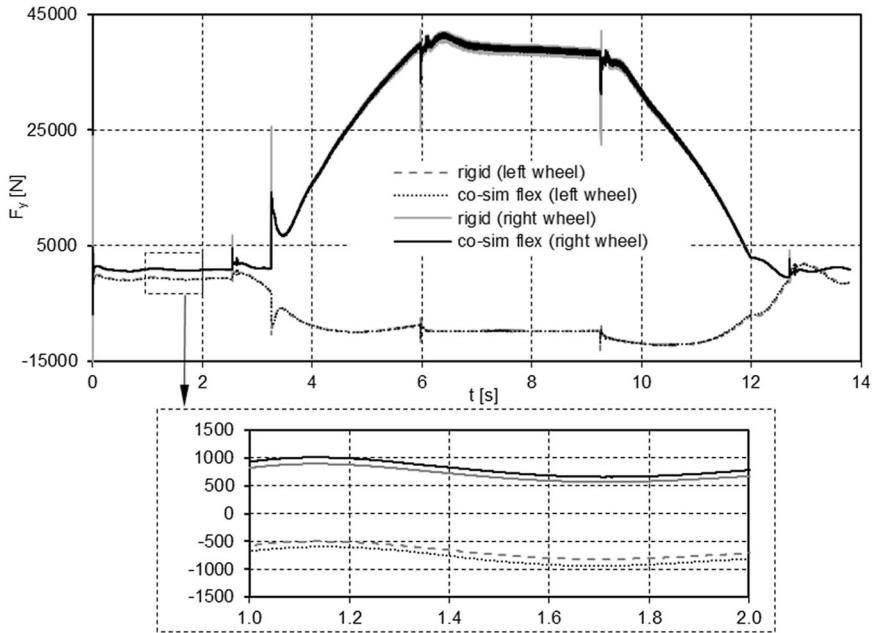


Fig. 20 Lateral forces applied on the left and right leading wheel

only occurs on the front right wheel of each bogie. Furthermore, it can be observed that on the same track position each wheel that passes perceives the position of the rail differently, which cannot be represented with a rigid track model. Moreover, the transversal track displacements on the straight segment are symmetric, i.e. the left and right rails move to the inside of the track. In contrast, on the curved segment both rails are displaced to the outer side of the curve being the right wheel displacement more prominent. This effect is also observed for the vertical displacements in the curved section where the outside rail is loaded heavily due to the curve negotiation and the track superelevation.

In the simulation of the railway vehicle–track interaction scenarios developed in this work, the simulation of the dynamics of the vehicle and track multibody model uses a variable time step integrator while a fixed time step of 2×10^{-5} s, used for the finite element flexible track model. This value for the time step is obtained by reducing the step size until the contact forces evaluated stabilize and converge, i.e. until they become identical for any time step smaller than that identified. It should also be noted that the co-simulation with rigid track and flexible track are respectively 7.9 and 57.3 times longer than that with the standalone multibody simulation with rigid track.

7 Conclusions

This work proposes a vehicle–track co-simulation methodology to allow the study of the coupled dynamics of the railway vehicle and the flexible track models. The key ingredient of the co-simulation is the wheel–rail interaction characterized by the rolling contact forces in which the contact detection problem is strongly influenced by the ability to evaluate the

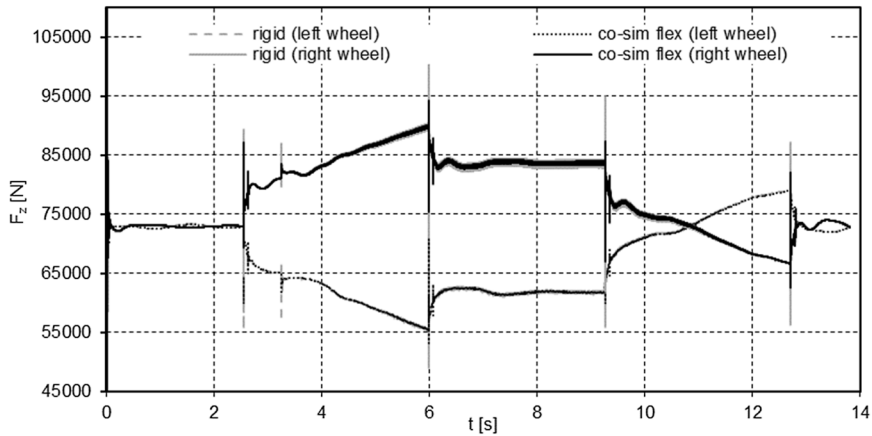


Fig. 21 Vertical forces applied on the left and right leading wheel

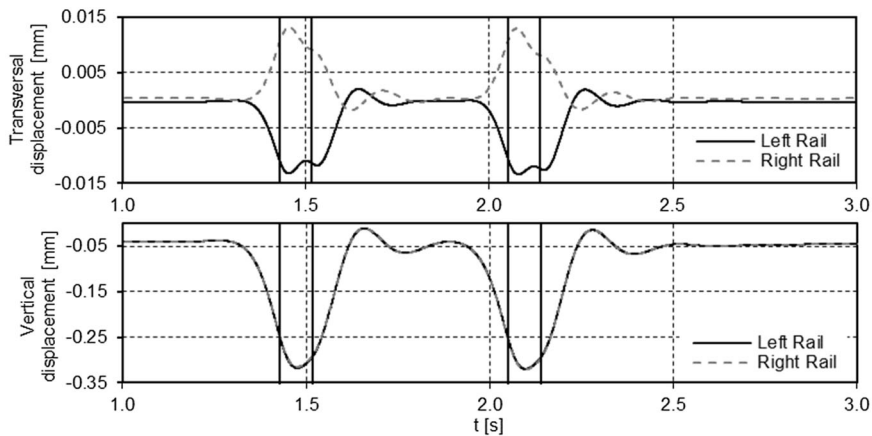


Fig. 22 Transversal and vertical displacements of the left and right rail at the 66 m mark of the track (straight track segment)

track deformation. The vehicle model is described and analyzed using a multibody dynamics model in which a variable time step integrator is used. The track model is described by a linear finite element method, in which a fixed time step integrator of the Newmark family is used. The wheel–rail contact force model is evaluated online with the Polach algorithm taking into account the deformation of the rails. The study of a case scenario allows us to identify some of the novel features of the methodology proposed here. Not only significant differences on the vehicle kinematics exist when considering the track flexibility, namely during curve negotiations, but also the contact forces are modified, the lateral, or creep, forces being higher for a flexible track. The track deformations are clearly identified, and closely related to the train wheelset kinematics, by using the methodology proposed. The results obtained do not allow understanding up to what extent the track flexibility influences the vehicle dynamics. Further studies on this aspect of the vehicle–track coupled dynamics can be carried as the interaction modeling procedure, via co-simulation, shows to be accurate and robust.

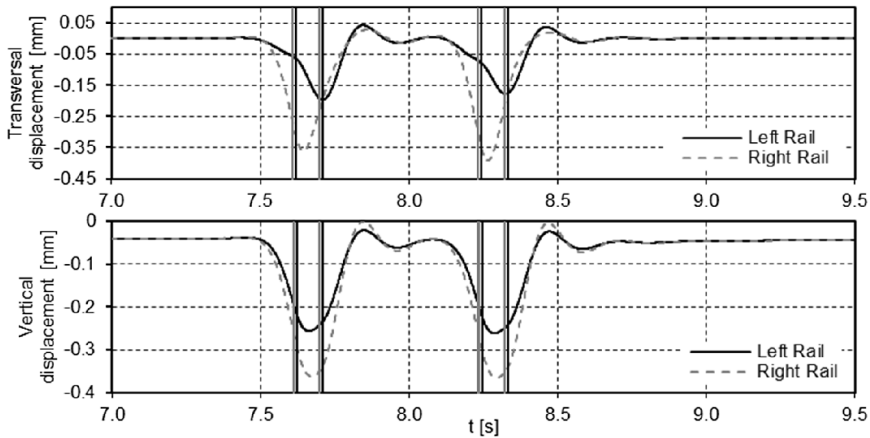


Fig. 23 Transversal and vertical displacements of the left and right rail at the 255 m mark of the track (curve track segment)

Publisher's Note Springer Nature remains neutral with regard to jurisdictional claims in published maps and institutional affiliations.

References

1. ERRAC: Strategic Rail Research Agenda 2020. Brussels, Belgium (2007)
2. OECD: Strategic Transport Infrastructure Needs to 2030. OECD Publishing, Paris (2012)
3. Felippa, C.A., Park, K.C.C., Farhat, C.: Partitioned analysis of coupled mechanical systems. *Comput. Methods Appl. Mech. Eng.* **190**, 3247–3270 (2001). [https://doi.org/10.1016/S0045-7825\(00\)00391-1](https://doi.org/10.1016/S0045-7825(00)00391-1)
4. Hulbert, G., Ma, Z.-D., Wang, J.: Gluing for dynamic simulation of distributed mechanical systems. In: Ambrósio, J. (ed.) *Advances on Computational Multibody Systems*, pp. 69–94. Springer, Dordrecht (2005)
5. Kubler, R., Schiehlen, W.: Modular simulation in multibody system dynamics. *Multibody Syst. Dyn.* **4**, 107–127 (2000)
6. Dietz, S., Hippmann, G., Schupp, G.: Interaction of vehicles and flexible tracks by co-simulation of multibody vehicle systems and finite element track models. *Veh. Syst. Dyn.* **37**, 372–384 (2002). <https://doi.org/10.1080/00423114.2002.11666247>
7. Heckmann, A., Arnold, M., Vaculín, O.: A modal multifield approach for an extended flexible body description in multibody dynamics. *Multibody Syst. Dyn.* **13**, 299–322 (2005). <https://doi.org/10.1007/s11044-005-4085-3>
8. Liu, F., Cai, J., Zhu, Y., Tsai, H.M., Wong, A.S.F.: Calculation of wing flutter by a coupled fluid-structure method. *J. Aircr.* **38**, 334–342 (2001). <https://doi.org/10.2514/2.2766>
9. Bathe, K.J., Zhang, H.: Finite element developments for general fluid flows with structural interactions. *Int. J. Numer. Methods Eng.* **60**, 213–232 (2004). <https://doi.org/10.1002/nme.959>
10. Naya, M., Cuadrado, J., Dopico, D., Lugin, U.: An efficient unified method for the combined simulation of multibody and hydraulic dynamics: comparison with simplified and co-integration approaches. *Arch. Mech. Eng.* **58**, 223–243 (2011). <https://doi.org/10.2478/v10180-011-0016-4>
11. Busch, M., Schweizer, B.: Coupled simulation of multibody and finite element systems: an efficient and robust semi-implicit coupling approach. *Arch. Appl. Mech.* **82**, 723–741 (2012). <https://doi.org/10.1007/s00419-011-0586-0>
12. Carstens, V., Kemme, R., Schmitt, S.: Coupled simulation of flow-structure interaction in turbomachinery. *Aerosp. Sci. Technol.* **7**, 298–306 (2003). [https://doi.org/10.1016/S1270-9638\(03\)00016-6](https://doi.org/10.1016/S1270-9638(03)00016-6)
13. Spreng, F., Eberhard, P., Fleissner, F.: An approach for the coupled simulation of machining processes using multibody system and smoothed particle hydrodynamics algorithms. *Theor. Appl. Mech. Lett.* **3**, 013005 (2013). <https://doi.org/10.1063/2.1301305>

14. Anderson, K.S., Duan, S.: A hybrid parallelizable low-order algorithm for dynamics of multi-rigid-body systems: Part I, chain systems. *Math. Comput. Model.* **30**, 193–215 (1999). [https://doi.org/10.1016/S0895-7177\(99\)00190-9](https://doi.org/10.1016/S0895-7177(99)00190-9)
15. Wang, J., Ma, Z., Hulbert, G.M.: A gluing algorithm for distributed simulation of multibody systems. *Nonlinear Dyn.* **34**, 159–188 (2003). <https://doi.org/10.1023/B:NODY.0000014558.70434.b0>
16. Verhoef, M., Visser, P., Hooman, J., Broenink, J.: Co-simulation of distributed embedded real-time control systems. In: Davies, J., Gibbons, J. (eds.) *Integrated Formal Methods: 6th International Conference, IFM 2007, Proceedings, Oxford, UK, July 2–5, 2007*, pp. 639–658. Springer, Berlin (2007)
17. Spiryagin, M., Simson, S., Cole, C., Persson, I.: Co-simulation of a mechatronic system using Gensys and Simulink. *Veh. Syst. Dyn.* **50**, 495–507 (2012). <https://doi.org/10.1080/00423114.2011.598940>
18. Gu, B., Asada, H.H.: Co-simulation of algebraically coupled dynamic subsystems without disclosure of proprietary subsystem models. *J. Dyn. Syst. Meas. Control* **126**, 1 (2004). <https://doi.org/10.1115/1.1648307>
19. Ambrósio, J., Pombo, J., Rauter, F., Pereira, M.: A memory based communication in the co-simulation of multibody and finite element codes for pantograph-catenary interaction simulation. In: Bottasso, C.L. (ed.) *Multibody Dynamics*, pp. 211–231. Springer, Dordrecht (2008)
20. Ambrósio, J., Pombo, J., Antunes, P., Pereira, M.: PantoCat statement of method. *Veh. Syst. Dyn.* **53**, 314–328 (2015). <https://doi.org/10.1080/00423114.2014.969283>
21. Massat, J.-P., Laurent, C., Bianchi, J.-P., Balmès, E.: Pantograph catenary dynamic optimisation based on advanced multibody and finite element co-simulation tools. *Veh. Syst. Dyn.* **52**, 338–354 (2014). <https://doi.org/10.1080/00423114.2014.898780>
22. Colombo, E.F., Di Gialleonardo, E., Facchinetti, A., Bruni, S.: Active carbody roll control in railway vehicles using hydraulic actuation. *Control Eng. Pract.* **31**, 24–34 (2014). <https://doi.org/10.1016/j.conengprac.2014.05.010>
23. Kuka, N., Verardi, R., Ariaudo, C., Dolcini, A.: Railway vehicle driveline modeling and co-simulations in SIMPACK-Simulink. In: *Proceedings of the Third International Conference on Railway Technology: Research, Development and Maintenance, Cagliari, Sardinia, Italy. Civil-Comp Press, Stirlingshire* (2016)
24. Knothe, K.L., Grassie, S.L.: Modelling of railway track and vehicle/track interaction at high frequencies. *Veh. Syst. Dyn.* **22**, 209–262 (1993). <https://doi.org/10.1080/00423119308969027>
25. Pombo, J., Ambrósio, J.: Application of a wheel–rail contact model to railway dynamics in small radius curved tracks. *Multibody Syst. Dyn.* **19**, 91–114 (2008)
26. Magalhaes, H., Ambrósio, J., Pombo, J.: Railway vehicle modeling for the vehicle–track interaction compatibility analysis. *Proc. Inst. Mech. Eng., Proc., Part K, J. Multi-Body Dyn.* **230**, 251–267 (2016). <https://doi.org/10.1177/1464419315608275>
27. Mazzola, L., Bruni, S.: Effect of suspension parameter uncertainty on the dynamic behavior of railway vehicles. In: *Uncertainty in Mechanical Engineering. Applied Mechanics and Materials*, vol. 104, pp. 177–185. Trans Tech Publ, Zurich (2012)
28. Polach, O., Evans, J.: Simulations of running dynamics for vehicle acceptance: application and validation. *Int. J. Railw. Technol.* **2**(4), 59–84 (2013). <https://doi.org/10.4203/ijrt.2.4.4>
29. Di Gialleonardo, E., Braghin, F., Bruni, S.: The influence of track modeling options on the simulation of rail vehicle dynamics. *J. Sound Vib.* **331**, 4246–4258 (2012). <https://doi.org/10.1016/J.JSV.2012.04.024>
30. Escalona, J.L., Sugiyama, H., Shabana, A.A.: Modelling of structural flexibility in multibody railroad vehicle systems. *Veh. Syst. Dyn.* **51**, 1027–1058 (2013). <https://doi.org/10.1080/00423114.2013.786835>
31. Lundqvist, A., Dahlberg, T.: Load impact on railway track due to unsupported sleepers. *Proc. Inst. Mech. Eng., F J. Rail Rapid Transit* **219**, 67–77 (2005). <https://doi.org/10.1243/095440905X8790>
32. Recuero, A.M., Escalona, J.L., Shabana, A.A.: Finite-element analysis of unsupported sleepers using three-dimensional wheel–rail contact formulation. *Proc. Inst. Mech. Eng., Proc., Part K, J. Multi-Body Dyn.* **225**, 153–165 (2011). <https://doi.org/10.1177/2041306810394971>
33. Johansson, A., Pålsson, B., Ekh, M., Nielsen, J.C.O., Ander, M.K.A., Brouzoulis, J., Kassa, E.: Simulation of wheel–rail contact and damage in switches and crossings. *Wear* **271**, 472–481 (2011). <https://doi.org/10.1016/j.wear.2010.10.014>
34. Martínez-Casas, J., Di Gialleonardo, E., Bruni, S., Baeza, L.: A comprehensive model of the railway wheelset–track interaction in curves. *J. Sound Vib.* **333**, 4152–4169 (2014). <https://doi.org/10.1016/J.JSV.2014.03.032>
35. Zhai, W., Wang, K., Cai, C.: Fundamentals of vehicle–track coupled dynamics. *Veh. Syst. Dyn.* **47**, 1349–1376 (2009). <https://doi.org/10.1080/00423110802621561>
36. Nikravesh, P.E.: *Computer-Aided Analysis of Mechanical Systems*. Prentice Hall, Englewood Cliffs (1988)
37. Ambrósio, J., Neto, A.: Stabilization methods for the integration of DAE in the presence of redundant constraints. *Multibody Syst. Dyn.* **10**, 81–105 (2003)

38. Gear, C.W.: Simultaneous numerical solution of differential-algebraic equations. *IEEE Trans. Circuit Theory* **18**, 89–95 (1971)
39. Przemieniecki, J.S.: *Theory of Matrix Structural Analysis*. McGraw-Hill, New York (1968)
40. Ambrósio, J., Antunes, P., Pombo, J.J.: On the requirements of interpolating polynomials for path motion constraints. In: Kecskeméthy, A., Geu Flores, F. (eds.) *Mechanisms and Machine Science*, pp. 179–197. Springer, Berlin (2015)
41. Pombo, J., Ambrósio, J.: An alternative method to include track irregularities in railway vehicle dynamic analyses. *Nonlinear Dyn.* **68**, 161–176 (2012)
42. Costa, J., Antunes, P., Magalhães, H., Ambrósio, J., Pombo, J.: Development of flexible track models for railway vehicle dynamics applications. In: Pombo, J. (ed.) *Proceedings of the Third International Conference on Railway Technology: Research, Development and Maintenance*. Civil-Comp Press, Stirlingshire (2016)
43. Hughes, T.: *The Finite Element Method: Linear Static and Dynamic Finite Element Analysis*. Prentice Hall, Englewood Cliffs (1987)
44. Bathe, K.-J.: *Finite Element Procedures*. Prentice Hall, Englewood Cliffs (1996)
45. Newmark, N.: A method of computation for structural dynamics. *J. Eng. Mech. Div.* **85**, 67–94 (1959)
46. Pombo, J., Ambrósio, J., Silva, M.: A new wheel–rail contact model for railway dynamics. *Veh. Syst. Dyn.* **45**, 165–189 (2007)
47. Lankarani, H.M., Nikravesh, P.E.: A contact force model with hysteresis damping for impact analysis of multibody systems. *J. Mech. Des.* **112**, 369–376 (1990)
48. Polach, O.: A fast wheel–rail forces calculation computer code. *Veh. Syst. Dyn.* **33**, 728–739 (1999)
49. Wen, Z., Wu, L., Li, W., Jin, X., Zhu, M.: Three-dimensional elastic–plastic stress analysis of wheel–rail rolling contact. *Wear* **271**, 426–436 (2011). <https://doi.org/10.1016/j.wear.2010.10.001>
50. Schweizer, B., Li, P., Lu, D., Meyer, T.: Stabilized implicit co-simulation methods: solver coupling based on constitutive laws (2015)
51. Quinn, M.J.: *Parallel Programming in C with MPI and OpenMP*. McGraw-Hill Higher Education, New York (2004)
52. Wilkinson, B., Allen, C.M.: *Parallel Programming: Techniques and Applications Using Networked Workstations and Parallel Computers*. Pearson/Prentice Hall, Upper Saddle River/New York (2005)
53. Downey, A.B.: The little book of semaphores. *Science* **80**(211), 1–291 (2009). <https://doi.org/10.1017/CBO9781107415324.004>
54. Li, D., Selig, E.T.: Method for railroad track foundation design. I: Development. *J. Geotech. Geoenviron. Eng.* **124**, 316–322 (1998). [https://doi.org/10.1061/\(ASCE\)1090-0241\(1998\)124:4\(316\)](https://doi.org/10.1061/(ASCE)1090-0241(1998)124:4(316))
55. SMARTRACK Project—System Dynamics Assessment of Railway Tracks: A Vehicle-Infrastructure Integrated Approach. FCT, PTDC/EME-PME/101419/2008 (2013)
56. CEN: EN 13674-1 Railway applications - Track - Rail - Part 1: Vignole railway rails 46 kg/m and above (2011)
57. Zhai, W., Wang, K., Cai, C.: Fundamentals of vehicle–track coupled dynamics. *Veh. Syst. Dyn.* **47**, 1349–1376 (2009). <https://doi.org/10.1080/00423110802621561>
58. Zhai, W.M., Wang, K.Y., Lin, J.H.: Modelling and experiment of railway ballast vibrations. *J. Sound Vib.* **270**, 673–683 (2004). [https://doi.org/10.1016/S0022-460X\(03\)00186-X](https://doi.org/10.1016/S0022-460X(03)00186-X)
59. Esveld, C.: Improved knowledge of CWR track. In: *Interact. Conf. Cost Eff. Saf. Asp. Railw. Track* (1998)
60. Magalhães, H.: Development of advanced computational models of railway vehicles. Master Thesis, Instituto Superior Técnico, Lisboa, Portugal (2013)
61. Costa, J.: Railway dynamics with flexible tracks. Master Thesis, Instituto Superior Técnico, Lisboa, Portugal (2015)